Investigation on Dynamic Behaviour of Condensation Heat Transfer in Indirective Evaporative Cooler

Yunran Min, Yi Chen*, Hongxing Yang

Renewable Energy Research Group, Research Institute for Sustainable Urban Development, The Hong Kong Polytechnic University, Hong Kong, China

*Corresponding author. E-mail address: cindy.chen@cpce-polyu.edu.hk (Y. Chen)

Abstract

Indirect Evaporative Cooling is a rapidly developing air-handling technology and has great application potentials for energy recovery in hot and humid regions. The condensation in dry channels of an indirect evaporative cooler (IEC) occurs when the dew point temperature of outdoor air is high. However, the dynamic heat transfer performance of an IEC during the process of condensation evolution was rarely discussed. This paper aims to experimentally investigate the dynamic behaviour of primary air condensation and its effects on the convective and total heat transfer rate of an IEC. A transparent cover plate is placed outside an aluminium heat exchanger plate to visualize the evolution process of droplets retained on the surface. The droplets falling frequency was recorded and the accumulated condensate mass was correlated based on an analytical method taking into account the contact angle and droplet volume. Results showed that the dynamic dehumidification performance can pose great influences on the convective heat transfer in IEC. The gradually diminished dropwise regions and increase of filmwise regions deteriorates the wet-bulb effectiveness of IEC by 14.8%. The convective heat flux keeps decreasing with the accumulation of condensate retention until a dynamic equilibrium is achieved between the retained and falling droplets.

Keywords: Indirect evaporative cooler; Dropwise condensation; Condensation evolution; Droplet behaviour; Heat transfer

Introduction

With the improvement of living standards, the demand for thermally comfortable indoor environments is increasing. Consequently, energy use for air-conditioning (A/C) has significantly increased over the last few decades. In 2017, 1.2 Mtoe energy was consumed and 3.7 million tons of carbon was discharged by A/C systems in Hong Kong [1]. With the growing population and increasing demands for building comfort, the energy demand for A/C will continue increasing.

Nowadays, the A/C market is dominated by Mechanical Vapour Compression Refrigeration (MVCR) systems [2], which use chillers relying on the reverse Rankine cycle. These systems cool the air to below its dew point and then dehumidify the cooled air to the desired state with the possible reheating process. The traditional A/C systems lead to intensive energy consumption, especially for treating hot and humid ambient air in subtropical areas like Hong Kong. To deal with the increasing energy consumption and global warming resulting from carbon emissions, many efforts have been made to develop alternative air cooling solutions by making use of natural and renewable energy resources [3]. The indirect evaporative cooling technology utilizes water evaporation to produce cooling air [4], which achieved higher energy efficiency and has gained fast development in recent decades [5-7].

In hot and humid regions, the indirect evaporative cooler (IEC) is proposed as an energy recovery unit for central A/C systems [8, 9], which captures the cooling potential from the exhaust air to pre-cool the fresh air. The core component in an IEC is the air-to-air heat exchanger which consists of alternative primary air and secondary air channels [10]. The cold and dry exhaust air from air-conditioned space is utilized as secondary air to enhance the evaporation of spraying water. Due to the large cooling capacity, the humid fresh air in the dry channels can be both cooled and dehumidified. Research showed that the condensation in dry channels has significant influences on the IEC cooling performance [11, 12]. Cui et.al [13] proposed a numerical model of a counter flow IEC in the presence of condensation from primary air. They found that the heat and mass transfer process in the IEC has been changed due to the occurrence of condensation. Chen et.al [14, 15] simulated the annual performance of a counter flow IEC applied in Hong Kong and indicated that the condensation states account for nearly half of the annual operation periods. Pandelidis et.al [16] identified several parameters that affect the condensation process and quantitatively analysed the impacts. The proposed model of IEC [16] was established based on ε-NTU method and solved by the modified Runge-Kutta method. Meng et.al [17] carried out a series of visualized experiments to investigate the turning point of IEC changing from a non-condensation state to partial or total condensation state under various inlet parameters. Previous studies on the model development of IEC with condensation are all based on the assumption of constant heat transfer coefficient for steady state. In the present study, the dynamic condensation heat transfer was investigated through an experimental study. Comparisons between the present study and other representative studies of IEC that involves the fresh air dehumidifying process are listed in Table 1.

Table 1. Comparison between the present study and some representative studies

Study	Chen et.al [15]	Lv et al. [18]	Present study
IEC type	Counter-flow plate-type IEC	Cross-flow IEC with corrugated aluminium plates	Cross-flow IEC with flat-type aluminium
Test conditions	Steady-state	Steady-state	Dynamic state
Proposed model	IEC model that neglects the thermal resistances of condensate water	Model on the average thickness of condensate film	Model on the volume of droplets on the plate surface
Observed condensation mode	-	filmwise	Droplet and filmwise
Measured parameters	Inlet and outlet air conditions	Inlet and outlet air conditions	Inlet and outlet air conditions, contact angle, droplet falling frequency

The dynamic behaviours of condensing droplets on the plate surface have significant influences on the performance of heat exchangers in terms of both sensible cooling and also dehumidification. With the fast development of advanced techniques on computer science, the evolution of condensation occurred in the heat exchangers can be explored by using the image recording and processing methods. Danilo et.al [19] investigated the influence of condensation on both convective and overall heat transfer rates. The condensation mechanism and droplets evolution process were addressed through experiments on the visualization of the condensation surface. Zhuang et al. [20] proposed a numerical model for simulating droplet behaviours that are governed by the coupling effect of gravity, surface tension and air flow. Key parameters for droplet movement were analysed including contact angles, air flow force, dew point temperature and water vapour partial pressure difference. Wang et.al [21] carried out an experimental study on the airside performance of the heat exchangers under dehumidifying conditions. The heat transfer performance was compared among different surfaces and results show that there is degradation on the heat transfer performance of the hydrophilic coating surface since the condensate flows along the fin surface. Eimann et.al [22] determined the thermal resistance of the condensate on the vertical channel walls through an experimental study. The temperature difference between the substrate surface and air-water interface can be examined using the infrared thermography, and the results were used to correlate the droplet heat transfer coefficients.

Although the additional latent heat released through the condensation process contributes to the energy saving of A/C systems by pre-dehumidification, it can deteriorate the sensible cooling performance of heat exchangers. Existing research about the IEC models in the presence of condensation from primary air only focuses on the steady-state heat and mass transfer characteristics. The energy and species conservation models were developed based on the assumption of constant heat transfer coefficient and neglected condensate water film. However, in reality, the growth of condensation on the plate surface of IEC could be a successive dynamic process. The condensate water retained on the surface can greatly

affect the sensible heat transfer in the primary air channels, especially during the evolution from dropwise condensation to filmwise condensation.

In this regard, the objective of this paper is to explore the dynamic condensation process and quantify the effect of primary air condensation on the convective heat transfer of IEC throughout the process of condensation evolution. The experimental apparatus of a cross-flow IEC was established which enables the visualization of condensation along with a vertical plate. An analytical approach was proposed to determine the accumulated condensate mass by combining droplet behaviours (i.e. contact angle, droplet volume) and measured outlet air conditions. Then, the dynamic dehumidification performance and the variation of convective heat transfer flux in the IEC were analysed along the condensation evolution process.

Experimental method

Experimental apparatus

The experimental bench was built in a laboratory with controllable indoor temperature and humidity. Fig. 1 presents the photo of the IEC test rig. A cross-flow heat exchanger which consists of alternative dry and wet channels was designed and fabricated. With the primary air flows in the horizontal direction in the dry channels, the secondary air is in counter-flow with the spraying water in the wet channels. As the secondary air evaporates the spraying water and takes the heat away, the humid primary air can be cooled below its dew point to condense the moisture. The schematic diagram of the tested IEC is shown in Fig. 2. To enable the visualization of condensate water film, the heat exchanger is equipped with a transparent plate cover facing the outermost primary air channel. The condensation growth and distribution can be recorded by a high-resolution camera placed in front of the viewing glass. The condensate water accumulated at the bottom of the heat exchanger can be drained through a 2° downward slope.

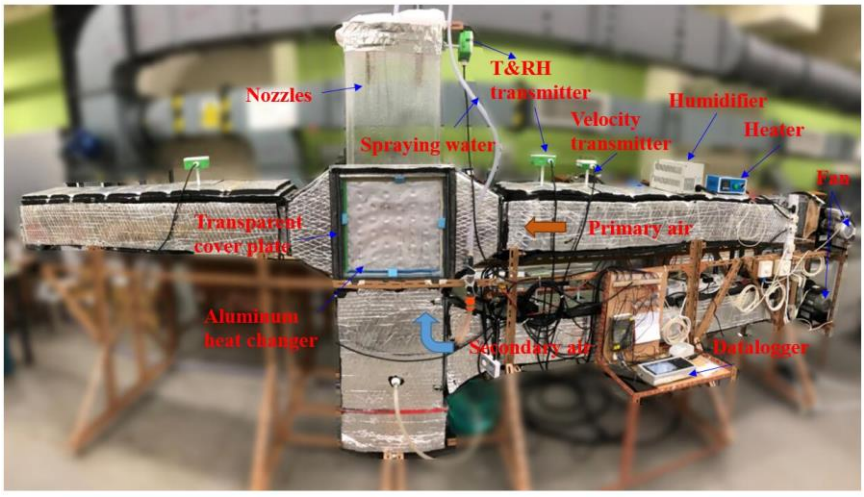

Fig. 1. Photo of the test rig

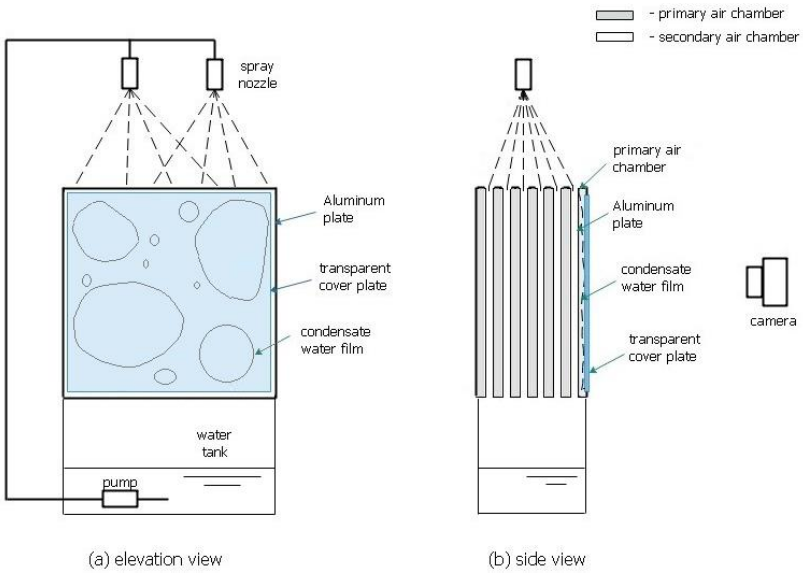

Fig. 2. The schematic diagram of the test rig

The primary and secondary air channels are separated by fabricated aluminium plates, and the detailed dimensions of the IEC heat exchanger are listed in Table 2. The inlet temperature and relative humidity of primary air were controlled by a heater and a humidifier installed in the air duct. The indoor air with a set temperature of 25℃ and relative humidity of 50% was used as the secondary air. The inlet and outlet air properties were measured by sensors and recorded by a data logger. The measurement instruments and specifications are shown in Table 3. The data collection interval for the acquisition system was set as 2s, and the image of the condensation was taken at 1 minute time interval. After the system started operation under certain inlet air parameters, the falling frequency of the droplets on the heat exchanger plate surface were measured continuously using a stopwatch. Due to the development of heat and mass transfer, the system took time to reach a steady-state with stable outlet air states. The steady-state in this study was defined as the outlet temperature and relative humidity variations are within 0.1°C and 1% for 5 min.

Table 2. Dimensions of the IEC heat exchanger module

Parameters	Value
Cooler length (L)	0.4 m
Cooler width (W)	0.2 m
Cooler height (H)	0.4 m
Channel gap (s)	4 mm
Number of channel pairs (n)	25
Plate thickness (δ)	0.15 mm

Table 3. Specification of different measuring instruments

Parameters	Device	Range	Accuracy
Dry bulb temperature	Pt1000 Model: EE160	-15 - 60℃	±0.3℃
Relative humidity	Pt1000 Model: EE160	10 - 95% RH	±2.5% RH
Air velocity	Hot film anemometer Model: EE65	0 - 10 m/s	±0.2 m/s
Power consumption	Power meter	0 - 10 A 0 - 2200 W	0.01 W

Uncertainty analysis

To determine the reliability of the experimental results, the uncertainties of the measured data and the calculated performance indicators have been analysed. The relative uncertainty of dependent variables were obtained using Eq. (1) [23]. Based on the operating condition of the tested IEC under steady-state, the uncertainty analysis results are listed in Table 4.

$$\frac{\Delta y}{y} = \left[\left(\frac{\partial f}{\partial x_1}\right)^2 \left(\frac{\Delta x_1}{y}\right)^2 + \left(\frac{\partial f}{\partial x_2}\right)^2 \left(\frac{\Delta x_2}{y}\right)^2 \cdots + \left(\frac{\partial f}{\partial x_n}\right)^2 \left(\frac{\Delta x_n}{y}\right)^2\right]^{\frac{1}{2}} \quad (1)$$

where Δy is the absolute uncertainty; $\Delta y/y$ is the relative uncertainty; f represents the function consisted of different independent variables, i.e. $x_1, \cdots x_n$; Δx is the absolute uncertainty of independent variables.

Table 4. Uncertainty analysis results

Parameter	Unit	Nominal value	Uncertainty
u_p	m/s	1.8	±4.3%
u_s	m/s	2.0	±3.9%
$t_{p,in}$	℃	30.3	±1.6%
$t_{p,out}$	℃	23.6	±1.4%
$\omega_{p,in}$	g/kg	21.7	±6.1%
$\omega_{p,out}$	g/kg	17.5	±2.8%
η_{wb}	-	0.54	±2.6%
q_{sen}	W/m^2	646	±6.9%
$\dot{m}_{fall}$	g/min	1.1	±2.8%
$m_{surf,n}$	g	11.6	±11.7%

To verify the accuracy of the measurement, the heat and mass balances in the IEC was examined between the primary air and secondary air. The influences of mass changes on the specific heat capacity of circulating spraying water and condensate water were neglected [24]. Specifically, the enthalpy

differences of the incoming and leaving air were derived from Eq.s (2) and (3) for primary air and secondary air respectively, as follows.

$$Q_p = m_p\left[c_{pa}\left(t_{p,in} - t_{p,out}\right) + h_{fg}\left(\omega_{p,in} - \omega_{p,out}\right)\right] \quad (2)$$

$$Q_s = m_s\left[c_{pa}\left(t_{s,out} - t_{s,in}\right) + h_{fg}\left(\omega_{s,out} - \omega_{s,in}\right)\right] \quad (3)$$

where, Q_p (kW) and Q_s (kW) are the heat transfer rates of primary air and secondary air respectively, c_{pa} (J/(kg·℃) is the specific heat of moist air, h_{fg} (kJ/kg) is the latent heat of vaporization of water, m_p (kg/s) and m_s (kg/s) are the mass flow rates of primary air and secondary air respectively, $t_{p,in}$ (℃) and $t_{p,out}$ (℃) are the inlet and outlet temperatures of primary air, $t_{s,in}$ and $t_{s,out}$ are the inlet and outlet temperatures of secondary air, $\omega_{p,in}$ (kg/kg) and $\omega_{p,out}$ (kg/kg) are the inlet and outlet moisture contents of primary air, $\omega_{s,in}$ (kg/kg) and $\omega_{s,out}$ (kg/kg) are the inlet and outlet moisture contents of secondary air.

The operating data during the steady-state were collected to compare the enthalpy changes between the two air streams. As shown in Fig. 3, discrepancies of experimental results were found to be within ±20%.

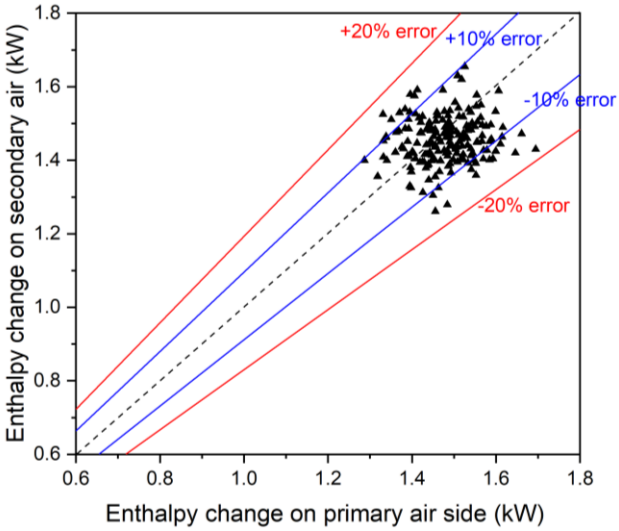

Fig. 3. Energy balance between the primary air and secondary air streams

Condensing droplet behaviours

Dynamic contact angle

The condensation flow pattern on a cold substrate generally depends on the wet properties of the solid surface, which is characterized as the contact angle under the thermodynamic equilibrium state. A larger contact angle can improve the droplet rolling and departure, which is favourable for achieving dropwise condensation with a heat transfer coefficient 5~7 times higher than that of filmwise condensation. A small contact angle makes the condensate droplets to cover a larger surface area and easy to form filmwise condensation. In order to obtain the contact angle of the plate surfaces, a small piece of

aluminium heat exchanger sample was measured by a contact angle meter (JCY20-13). The static contact angle on the horizontal surface was tested to be 78°.

The equilibrium contact angle (θ) for a drop on inclined planes can be expressed as a third-order polynomial in the form of an azimuthal angle, advancing contact angle (θ_{adv}) and receding contact angle (θ_{rec}). As shown in Fig. 4b, the advancing and receding contact angle were measured on a vertical surface and was used to assess the total volume of a single droplet by two-circle method [25]. In the IEC, the air flow force also has effects on contact angles of condensation droplets, leading to a deviation angle (χ) between the vertical direction and the actual droplet movement direction. As shown in Fig. 4a, the deviation angle was measured to be 6° under the primary air velocity of 1.8 m/s. Considering the actions of air flow force (F_a), gravity (G) and surface tension (F_s), the contact angle for the droplet is given by Eq. (4) [26].

$$cos\theta = 2\frac{cos\theta_{adv} - cos\theta_{rec}}{\pi^3}(\varphi - \chi)^3 - 3\frac{cos\theta_{adv} - cos\theta_{rec}}{\pi^2}(\varphi - \chi)^2 + cos\theta_{adv} \quad (4)$$

where φ is the azimuthal angle, the θ_{adv} and θ_{rec} on aluminium heat exchanger plate of the IEC were measured to be 85° and 42°, respectively. The deviation angle (χ) of droplet motion was obtained through the visualized primary air channel in the IEC test rig.

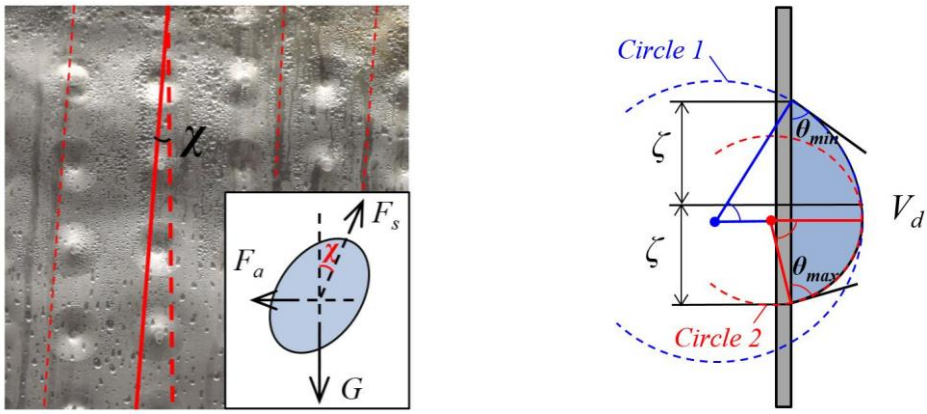

(a) deviation angle of droplet motion (b) volume and radius of a single droplet

Fig. 4. The profile of a single droplet on the plate surface

Droplet volume

The droplets attached to the vertical plate surface do not have a regular shape of a spherical cap after growing and merging. To estimate the total volume of droplets, there are two assumptions: the droplets departure diameter (D_d) can be fitted by surface tension and contact angle as specified in Eq. (5) [27], and the volume of a single droplet (V_d) can be obtained by integrating a function of contact angle (θ) and contour radius (ζ) over cross sections taken at all azimuthal angles (φ). For a droplet on the inclined

surface, the contour is an ellipse with a radius at symmetry plane larger than the equivalent diameter of base contour. As a result, the equivalent departure diameter needs to be converted to contour radius [28]. The two-circle method (as shown in Fig. 4b) performed by Elsherbini and Jacobi [25] was used to assess the contour radius and total volume of a single droplet on vertical surfaces, expressed as Eq. (6) and (8).

$$D_d = \left[\left(\frac{\sigma_l}{\rho_l g}\right)\cdot\left(\frac{16sin^3\theta_M}{2\theta_M - \sin(2\theta_M)}\right)\cdot sin\left(\frac{\theta_{adv}-\theta_{rec}}{2}\right)\right]^{\frac{1}{2}} \quad (5)$$

$$\zeta(\varphi) = \frac{D_d}{2}\sqrt{\frac{1+0.096Bo}{cos^2\varphi + (1+0.096Bo)^2 sin^2\varphi}} \quad (6)$$

$$Bo = \frac{\rho_l g D_d^2 sin\alpha}{\sigma_l} \quad (7)$$

$$V_d \approx \int f(\zeta(\varphi), \theta(\varphi))\, d\varphi \quad (8)$$

where σ_l is the water surface tension which is set to be 73.7×10^{-3} N/m, θ_M is the mean contact angle which is calculated by: $\theta_M = (\theta_{adv} + \theta_{rec})/2$, *Bo* is the Bond number which represents the ratio of gravitational to surface tension forces, α is the surface inclination angle which is 90° for vertical plates.

Performance evaluation index

The condensation from primary air can enhance the overall heat transfer, while weakens the convective heat transfer to some extent. To understand the heat and mass transfer mechanisms throughout the condensation process, it is essential to analyse the influence of primary air condensation on convective heat transfer performance of the IEC. In this study, the convective and latent heat transfer were calculated separately by combining the experimental data and empirical correlations on dropwise condensation.

Convective heat transfer

In an IEC, the primary air flow in the dry channels is cooled by the cold plates. However, the water vapour in the moist air could condense when the temperature of the plate wall adjacent to the primary air is below the dew point temperature. The small droplets are formed and retained on the surface which deteriorates the convective heat transfer process.

Two evaluation indexes were used in order to analyse the effect of condensate mass on the heat transfer performance of the IEC. The wet-bulb effectiveness (η_{wb}) is usually used as an evaluation index to describe the performance of IEC for sensible cooling, as calculated in Eq. (9).

$$\eta_{wb} = \frac{t_{p,in} - t_{p,out}}{t_{p,in} - t_{wb,s}} \quad (9)$$

where, $t_{wb,s}$ is the wet-bulb temperature of secondary air at inlet.

During the condensation process, the inlet and outlet primary air temperature and moisture were recorded during the operating time. Energy balance can be achieved as described in Eq. (10). The overall heat transfer rate (q_{tot}, kW) on the plate surface, which involves both the convective heat and mass transfer, is equal to the enthalpy difference of primary air at inlet and outlet. By considering the heat balance between the primary air and plate surface, the convective heat transfer flux (q_{sen}, kW/m^2) of the primary air can be expressed by Eq. (11).

$$q_{tot} = q_{sen} + q_{lat} = m_p c_{pa}\left(t_{p,in} - t_{p,out}\right) \cdot \frac{u_p}{L} + m_p h_{fg}\left(\omega_{p,in} - \omega_{p,out}\right) \cdot \frac{u_p}{L} \quad (10)$$

$$q_{sen} = \frac{Q_{sen}}{A} = c_{pa} m_p \left(t_{p,in} - t_{p,out}\right) \cdot \frac{u_p}{AL} \quad (11)$$

where, u_p (m/s) is the primary air flow velocity, L (m) is the length of heat exchanger, A (m^2) is the area of heat exchanger plate.

Dehumidification performance

Based on the mass balance, the moisture difference between primary air at inlet and outlet of the IEC is equal to the mass of condensate water (Δm_c) through the dehumidifying process, as shown in Eq. (12). The condensate water will retain on the plate surface by forming droplets due to the surface tension, however, droplets could fall off to the bottom of the channel and be drained away when growing up to the departure size. The mass of fall-off droplets ($\dot{m}_{fall}$) is integrated from the mass of a single droplet and the falling frequency measurement, as shown in Eq. (13). During the evolution process of primary air condensation, the droplets falling frequency on the plate surface could vary with the time, and the mass balance between accumulated condensate water, droplets fall-off and droplets retained on the plate surface can be expressed in Eq. (14). The mass of condensate water retained on the plate surface at a certain moment ($m_{surf,n}$) can be obtained using Eq. (15).

$$\Delta m_c = m_a \cdot \left(\omega_{p,in} - \omega_{p,out}\right) \quad (12)$$

$$\dot{m}_{fall} = \rho_l \cdot f_d \cdot V_d \quad (13)$$

$$\sum_{\tau=0}^{\tau=n} \Delta m_c = m_{surf,n} + \sum_{\tau=0}^{\tau=n} \dot{m}_{fall} \quad (14)$$

$$m_{surf,n} = \sum_{\tau=0}^{\tau=n} m_a \cdot \left(\omega_{p,in} - \omega_{p,out}\right) - \rho_l V_d \cdot \sum_{\tau=0}^{\tau=n} f_d \quad (15)$$

where, f_d (min^{-1}) is the droplets falling frequency in one minute and was counted during the experiments. m_a (kg/min) is the mass flow rate of the primary air. τ (min) is the time unit which varies from 0 to 30 according to the experimental duration.

Results and discussion

In order to investigate the transient performance of cross-flow IEC during the condensation evolution in the primary air channels, a case study was carried out under a typical operating scenario in hot and

humid areas with the inlet primary air and secondary air conditions listed in Table 5. For IEC applications in real buildings, the condensation of primary air could occur only when the fresh air is humid and the secondary air is cold and dry. In hot and humid areas, the exhaust air from air-conditioned space is used as secondary air in the IEC, which has a relatively stable temperature and relative humidity. In this study, the design condition of the case study was determined based on the indoor comfort zone and typical summer conditions for hot and humid climate areas.

Table 5. Operating conditions for a case study

Parameters	Symbol	Value
Inlet primary air temperature (℃)	$t_{p,in}$	30
Inlet primary air relative humidity (%)	$RH_{p,in}$	80
Inlet primary air velocity (m/s)	u_p	1.8
Inlet secondary air temperature (℃)	$t_{s,in}$	25
Inlet secondary air relative humidity (%)	$RH_{s,in}$	50
Inlet secondary air velocity (m/s)	u_s	2

Visualized condensation growth

From the captured images on the heat exchange plate surface over time, as shown in Fig. 5, the evolution of condensation taken place in the IEC was observed from the nucleation, growth, to a dynamic steady state with relatively stable droplets falling frequency. As shown in Fig. 5(a), the moisture begins to converge on the plate surface with the droplet nucleation process and they keep growing to larger droplets. In Fig. 5(b), the maximum droplet began to fall-off as a rivulet on the plate surface at 7th minute. The downward slope at the bottom of the air channels can drain the condensate water in the case of channel block by condensate accumulation. In Fig. 5(c), the amount of falling droplets increases as more and more droplets grow to the departure size. The updated condensate regions wiped by the falling droplets allow the re-nucleation of new droplets to repeat the droplet growth and departure cycle. When the condensation is fully developed with the rivulets continuously appearing on the whole surface as shown in Fig. 5(d), a dynamic steady state of the heat and mass transfer in the IEC can be reached with relatively stable condensation rate and outlet air states. The different droplet growth rates on the surface can be attributed to the uneven distribution of the plate surface temperature in cross-flow arrangement.

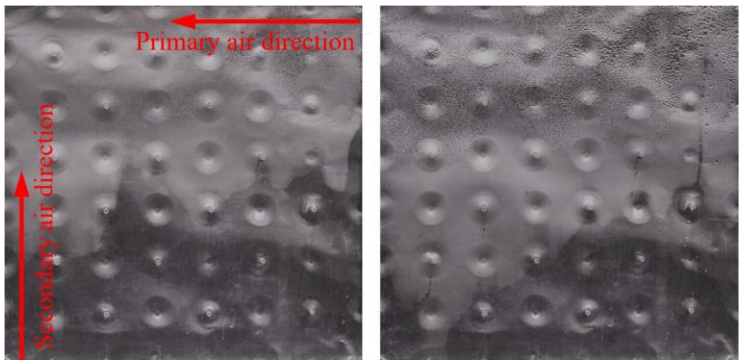

(a) 4 min (b) 7 min

(c) 12 min (d) 20 min

Fig. 5. Evolution of condensation on the plate surface of IEC

Dynamic performance of outlet air properties

Under dehumidifying conditions, the evolution of the condensation on the plate surface of IEC developed through a dynamic process. As shown in Fig. 6, the inlet moisture content of primary air keeps increasing after switching on the humidifier. After the inlet moisture maintained at 21.5 g/kg at t =150s, the outlet primary air still increased before reaching the steady-state at 17.7 g/kg. The moisture difference between inlet and outlet primary air reached a peak of 6.0 g/kg during the initial test period. With the growth of condensation, the condensate water was retained on the plate surface and increased the thermal resistance of heat transfer. As a result, the dehumidification process slowed down, and the moisture content difference gradually decreased to 3.8 g/kg with the highest reduction rate of 37%. The uncertainty of the measured humidity ratio of inlet and outlet primary air was 2.8% and 6.1%, respectively. The uncertainty of the moisture content difference under steady-state was calculated as 6.7%.

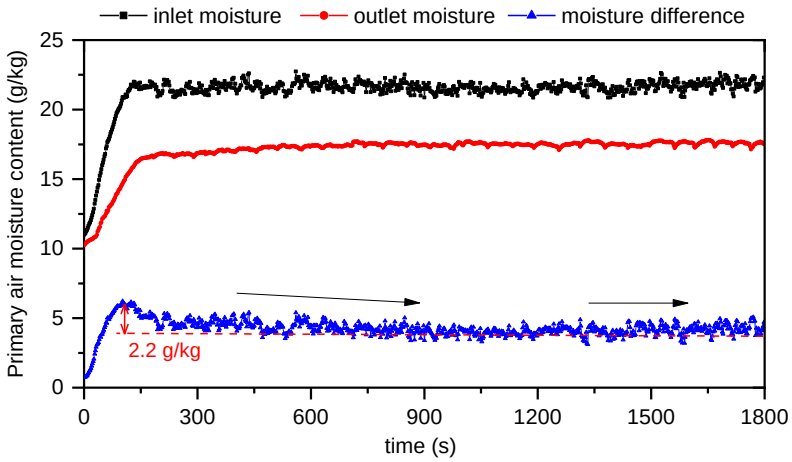

Fig. 6. Variation of outlet primary air moisture and dehumidifying performance of IEC over time

Fig. 7 shows the variation of inlet and outlet primary air temperature during the test duration of 30 minutes after switching on the system. The inlet primary air temperature was increased rapidly to 30℃ as soon as the heater was turned on. After the inlet temperature was maintained at 30℃, the outlet temperature of primary air gradually increased from 22.7 to 23.5℃ until a steady state was reached after 15 minutes. Two reasons can be attributed to the rise of outlet primary air temperature during the condensation process. Firstly, the latent heat released through humid air condensation could increase the plate surface temperature for cooling. Secondly, the transition of condensation modes on the plate surface from dropwise to filmwise largely reduced the overall heat transfer coefficient.

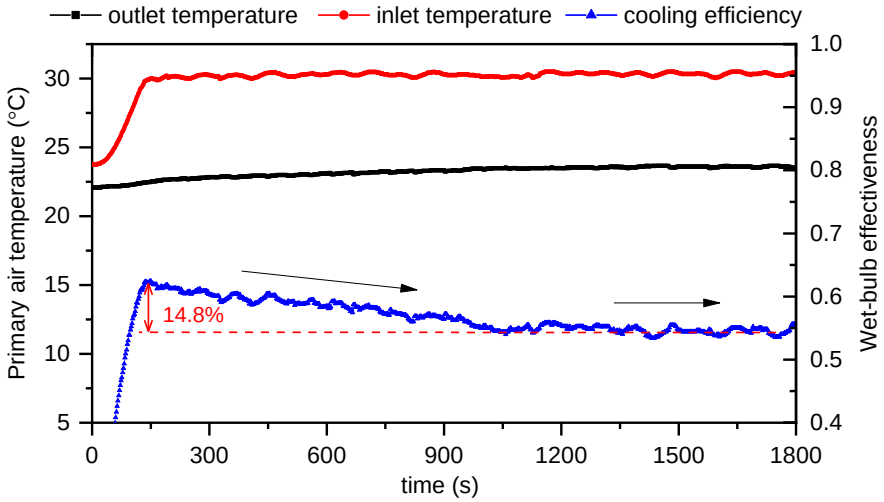

Fig. 7. Variation of outlet primary air temperature and wet-bulb effectiveness of IEC over time

The decreased temperature drop of primary air indicates the reduction of the wet-bulb effectiveness (η_{wb}) of the IEC, as shown in Fig. 7. Firstly, the value of η_{wb} peaked at 0.62 with the increase of air temperature dropped after turning on the system. Then, it shows a downward trend in η_{wb} by around 14.8% for 15 minutes until its value remains stable at 0.54. The uncertainty of the wet-bulb effectiveness

under steady-state was calculated as 2.6% based on the absolute uncertainty of measured temperatures. During the initial test period, the condensation on the plate surface was mainly in the dropwise form which enlarges the heat transfer area and benefits the heat transfer performance. However, as the droplets growing up to the departure size, the rivulets would occur and wipe away the neighbouring drops by forming condensate water films. The gradually diminished dropwise condensation and increased filmwise condensation on the plate surface could deteriorate the overall heat transfer due to the higher thermal resistance of the thick water film.

The dynamic process of primary air and secondary air handling in the IEC was plotted in a psychometric chart, as shown in Fig. 8. The primary air was cooled by the heat exchanger plate with the extracted moisture, and generates the condensate droplets adhered to the channel walls. At 150s, the heat transfer rate of the primary air flow was 1.71 kW, and the outlet primary air was treated to a state point with lower temperature and humidity ratio than the outlet primary air at 1800s. Due to the increasing condensation that forms a water film and deteriorates the heat transfer, the average heat transfer rate of the primary air under the steady-state (at 1800s) was reduced to 1.48 kW.

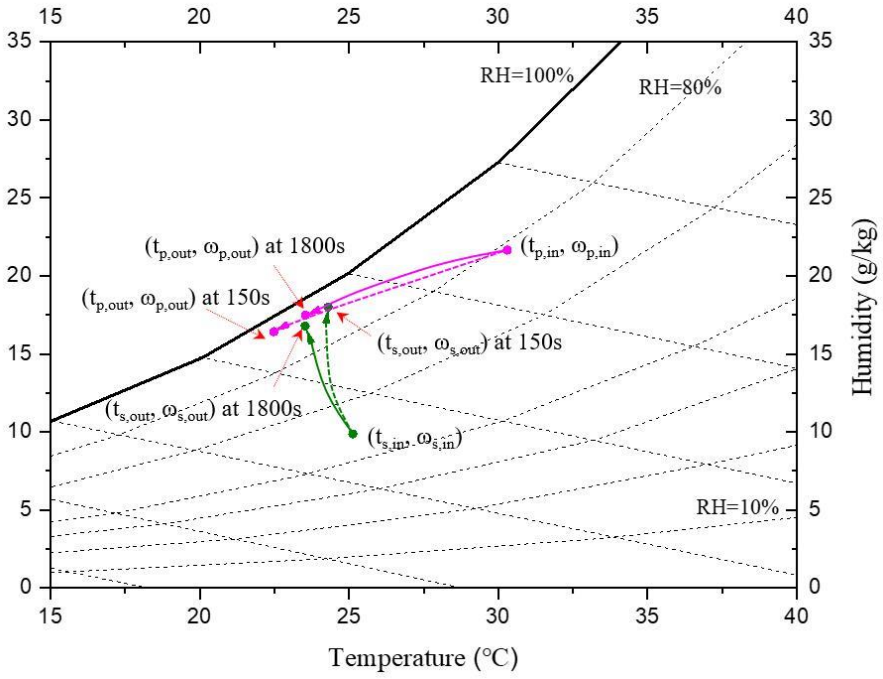

Fig. 8. Primary air and secondary air handling process at 150 s and 1800 s

Accumulated dehumidification performance

During the evolution of primary air condensation, the droplets formed on the plate surface have a wide range of falling frequency. Fig. 9 shows the variation of condensate mass and its effect on the convective heat flux density of the IEC under the dynamic dehumidifying conditions. The droplets begin to fall off from the plate surface at t =7min, and then the accumulated mass of falling droplets rises continuously.

An increasing upward trend was observed on the droplets falling frequency from 3/min to 10/min for 7 min ≤ t ≤ 18 min, followed by a linear relationship with time after t = 18 min. In contrast, the mass of droplets retained on the plate surface increased rapidly during the initial operating period (t ≤ 7min). With the departure of droplets emerged at t = 7 min, the condensate mass on the plate surface started to grow slowly and ultimately maintained at a certain value at t = 18 min.

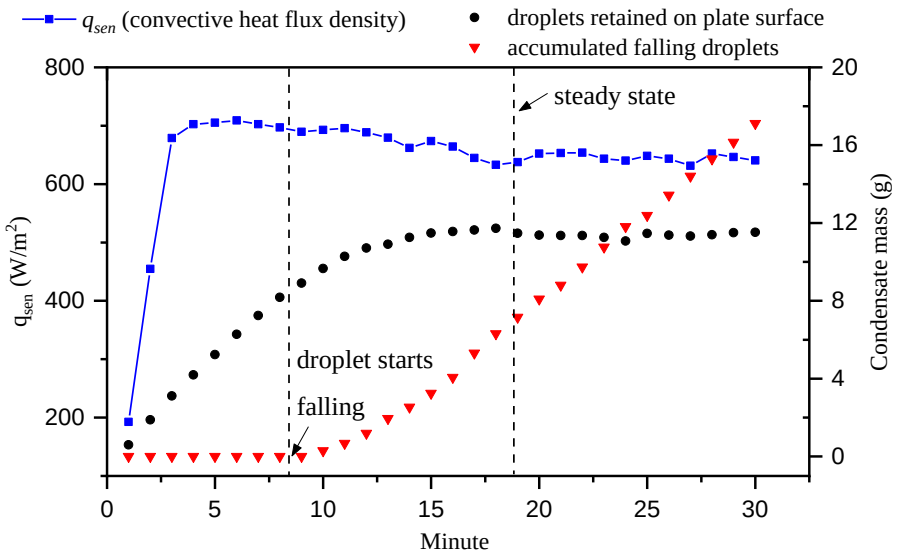

Fig. 9. Accumulated dehumidification performance and convective heat transfer flux of IEC

Fig. 9 shows that the variation of convective heat transfer flux is closely related to the condensate mass retained on the plate surface. The inlet primary air temperature was increased rapidly after turning on the heater, which led to a sharp rise in the convective heat transfer flux. After the inlet air temperature was maintained at the set point, the convective heat transfer was relatively stable for 3min ≤ t ≤ 7min. During this process, the condensate water was gathered on the plate surface in the form of dropwise which enlarged the heat transfer areas. However, the droplets grew through coalescence instead of direct condensation after the droplet size was larger than a certain value [29], which had inversely reduced the heat transfer areas. At t =7min, the large droplet started to fall off from the plate surface. The decline in the convective heat transfer flux became more apparent due to the transition from dropwise condensation to filmwise condensation. The convective heat transfer flux continued to fall due to the additional thermal resistance of water film with the accumulation of condensate mass retained on the plate surface. A dynamic steady state was achieved at t =18min with relatively stable droplets falling frequency. The convective heat transfer flux varied within a very small range around 646 W/m^2 after t =18min, with the condensate mass retained on the plate surface being maintained at 11.6 g. In sum, when the IEC was operated under dehumidifying conditions, the variation of convective heat transfer flux was inversely correlated to the condensate retention affected by the droplet behaviours on the plate surface.

Conclusions

The present study focuses on the condensation evolution of primary air in the indirect evaporative cooler (IEC) under dehumidifying conditions. A dedicated experimental set up was established to observe the dynamic condensation process and collect the test data on transient heat transfer performance. The accumulated condensate mass was determined by using measured data and an analytical method of droplet behaviours. The influences of accumulated condensate mass on the convective heat flux were analysed. From the condensation visualization and measured data on the thermodynamic performance of the tested IEC, the following conclusions can be drawn:

(1) The evolution of the condensation on the plate surface of IEC experiences a dynamic process from nucleation, growth, to departure. The moisture converges on the plate surface to form droplets. As the droplet grows to the departure size, a rivulet would occur and wipe away the neighbouring drops by forming condensate water films. The dropwise condensation would gradually become diminished with the increase of filmwise until a steady state is reached with stable droplets falling frequency.

(2) The condensate water is gradually accumulated and retained on the plate surface, increasing the thermal resistance. During the test, the moisture difference between inlet and outlet primary air reached a peak of 6.0 g/kg and then decreased to 3.8 g/kg along with the growth of condensation. Also, the outlet temperature of primary air gradually increased from 22.7 to 23.5℃, indicating a 14.8% reduction of wet-bulb effectiveness.

(3) The variation of convective heat transfer flux (q_{sen}) is inversely correlated to the condensate mass that retained on the plate surface (m_{surf}). During the droplet nucleation process, there is no falling droplet and the q_{sen} was shown to level off. When the droplet falling frequency was increased from 3/min to 10 /min, the q_{sen} was continued to decline with a rise of m_{surf}. A steady-state was ultimately achieved with a stable q_{sen} until the m_{surf} reached a dynamic equilibrium.

The results of this study provide a better understanding of the surface characteristics and to improve the performance of IEC under dehumidifying conditions. The enhancement of convective heat transfer in IEC can be achieved by modifying the surface materials to reduce the condensate mass retained on the plate surface. For future study, the hydrophobic coating can be applied to the plate surfaces in the dry channels of IEC for offering better condensate drainage performance.

AUTHOR′S CONTRIBUTION

Yunran Min conducted the experimental study and data analysis of the research presented. Yi Chen and Hongxing Yang initialized this study and supervised the model development.

STATEMENTS OF CONFLICT OF INTERESTS

The authors declare that they have no known competing financial interests or personal relationships that could have appeared to influence the work reported in this paper.

ACKNOWLEDGEMENT

The authors wish to acknowledge the financial supports from the General Research Fund of the Hong Kong SAR Government and the studentship provided by the Research Institute of Sustainable Urban Development (RISUD) of The Hong Kong Polytechnic University (1-ZVDR).

REFERENCES

1. Government of Hong Kong SAR, Electrical and Mechanical Services Department (EMSD). Hong Kong Energy End-use Data, https://www.emsd.gov.hk/filemanager/en/content_762/HKEEUD2019.pdf (2019), [26 June 2020].
2. Arun BS and Mariappan V. Experimental study of an ultrasonic regenerative evaporative cooler for a desiccant cooling system. Building Services Engineering Research and Technology 2018; 40: 151-175. DOI: https://10.1177/0143624418810934 .
3. Robinson D, Lomas KJ, Cook MJ, Eppel, H. Passive down-draught evaporative cooling: Thermal modelling of an office building. Indoor and Built environment 2004; 13: 205-221. DOI: https://doi.org/10.1177/1420326X04043816.
4. Englart S. Use of a membrane module for semi-direct air evaporative cooling. Indoor and Built Environment, Online epubl 24 September 2019: 1420326X19877510. DOI: https://10.1177/1420326X19877510.
5. Maheshwari G, Al-Ragom F and Suri R. Energy-saving potential of an indirect evaporative cooler. Applied Energy 2001; 69: 69-76. DOI: https://doi.org/10.1016/S0306-2619(00)00066-0.
6. Delfani S, Esmaeelian J, Pasdarshahri H, Karami, M. Energy saving potential of an indirect evaporative cooler as a pre-cooling unit for mechanical cooling systems in Iran. Energy and Buildings 2010; 42: 2169-2176. DOI: https://doi.org/10.1016/j.enbuild.2010.07.009.
7.Jaber S and Ajib S. Evaporative cooling as an efficient system in Mediterranean region. Applied Thermal Engineering 2011; 31: 2590-2596. DOI: https://doi.org/10.1016/j.applthermaleng.2011.04.026.
8.Guo C, Liu Q, Zheng B, You Y, Li Y. Development of model based on condensation area ratio and effect on heat transfer capacity of indirect evaporative cooling. Applied Thermal Engineering 2020; 164: 114557. DOI: https://doi.org/10.1016/j.applthermaleng.2019.114557.
9.Min Y, Chen Y and Yang H. A statistical modeling approach on the performance prediction of indirect evaporative cooling energy recovery systems. Applied Energy 2019; 255: 113832. DOI: https://doi.org/10.1016/j.apenergy.2019.113832.
10.Kim MH, Kim JH, Kwon OH, Choi AS, Jeong J. Energy conservation potential of an indirect and direct evaporative cooling assisted 100% outdoor air system. Building

Services Engineering Research and Technology 2011; 32: 345-360. DOI: https://doi.org/10.1177/0143624411402637.
11. Zheng B, Guo C, Chen T, Lv J, You Y. Development of an experimental validated model of cross-flow indirect evaporative cooler with condensation. Applied Energy 2019; 252: 113438. DOI: https://doi.org/10.1016/j.apenergy.2019.113438.
12. Min Y, Chen Y and Yang H. Numerical study on indirect evaporative coolers considering condensation: A thorough comparison between cross flow and counter flow. International Journal of Heat and Mass Transfer 2019; 131: 472-486. DOI: https://doi.org/10.1016/j.ijheatmasstransfer.2018.11.082.
13. Cui X, Mohan B, Islam MR, Chua KJ. Investigating the energy performance of an air treatment incorporated cooling system for hot and humid climate. Energy and Buildings 2017; 151: 217-227. DOI: https://doi.org/10.1016/j.enbuild.2017.06.059.
14. Chen Y, Yang H and Luo Y. Indirect evaporative cooler considering condensation from primary air: Model development and parameter analysis. Building and Environment 2016; 95: 330-345. DOI: https://doi.org/10.1016/j.buildenv.2015.09.030.
15. Chen Y, Yang H and Luo Y. Parameter sensitivity analysis and configuration optimization of indirect evaporative cooler (IEC) considering condensation. Applied Energy 2017; 194: 440-453. DOI: https://doi.org/10.1016/j.apenergy.2016.06.121.
16. Pandelidis D, Cichoń A, Pacak A, Anisimov S, Drąg P. Performance comparison between counter- and cross-flow indirect evaporative coolers for heat recovery in air conditioning systems in the presence of condensation in the product air channels. International Journal of Heat and Mass Transfer 2019; 130: 757-777. DOI: https://doi.org/10.1016/j.ijheatmasstransfer.2018.10.134.
17. Meng D, Lv J, Chen Y, Li H, Ma X. Visualized experimental investigation on cross-flow indirect evaporative cooler with condensation. Applied Thermal Engineering 2018; 145: 165-173. DOI: https://doi.org/10.1016/j.applthermaleng.2018.09.026.
18. Lv J, Meng D, Chen Y, You Y, Li H. An experimental study on condensate film of indirect evaporative cooler. Energy Procedia 2019; 158: 5753-5758. DOI: https://doi.org/10.1016/j.egypro.2019.01.556.
19. Danilo S, Dominique C and Frédéric P. Experimental dropwise condensation of unsaturated humid air – Influence of humidity level on latent and convective heat transfer for fully developed turbulent flow. International Journal of Heat and Mass Transfer 2016; 102: 846-855. DOI: https://doi.org/10.1016/j.ijheatmasstransfer.2016.06.001.
20. Zhuang D, Ding G, Hu H, Fujino H, Inoue S. Condensing droplet behaviors on fin surface under dehumidifying condition Part I: Numerical model. Applied Thermal Engineering 2016; 105: 336-344. DOI: https://doi.org/10.1016/j.applthermaleng.2015.02.082.
21. Wang C C, Lee W S, Sheu W J, Chang Y J. A comparison of the airside performance of the fin-and-tube heat exchangers in wet conditions; with and without hydrophilic coating. Applied Thermal Engineering 2002; 22: 267-278. https://doi.org/10.1016/S1359-4311(01)00090-4.
22. Eimann F, Zheng S, Philipp C, Fieback T, Gross U. Convective dropwise condensation out of humid air inside a horizontal channel – Experimental investigation of the condensate heat transfer resistance. International Journal of Heat and Mass Transfer 2018; 127: 448-464. DOI: https://doi.org/10.1016/j.ijheatmasstransfer.2018.08.015.
23. Coleman HW and Steele WG. Experimentation, validation, and uncertainty analysis for engineers. New York: John Wiley & Sons, 2018.
24. Duan Z, Zhan C, Zhao X, Dong X. Experimental study of a counter-flow regenerative evaporative cooler. Building and Environment 2016; 104: 47-58. DOI: https://doi.org/10.1016/j.buildenv.2016.04.029.

25. ElSherbini A and Jacobi A. Liquid drops on vertical and inclined surfaces: II. A method for approximating drop shapes. Journal of colloid and interface science 2004; 273: 566-575. DOI: https://doi.org/10.1016/j.jcis.2003.12.043.
26. Zhuang D, Hu H, Ding G, Xi G, Han W. Numerical model for liquid droplet motion on vertical plain-fin surface. HVAC&R Research 2014; 20: 332-343. DOI: https://doi.org/10.1080/10789669.2014.890460.
27. Min J and Webb RL. Condensate formation and drainage on typical fin materials. Experimental Thermal and Fluid Science 2001; 25: 101-111. DOI: https://doi.org/10.1016/S0894-1777(01)00062-0.
28. ElSherbini A and Jacobi A. Liquid drops on vertical and inclined surfaces: I. An experimental study of drop geometry. Journal of colloid and interface science 2004; 273: 556-565. DOI: https://doi.org/10.1016/j.jcis.2003.12.067.
29. Chen X and Derby MM. Droplet departure modeling and a heat transfer correlation for dropwise flow condensation in hydrophobic mini-channels. International Journal of Heat and Mass Transfer 2018; 125: 1096-1104. DOI: https://doi.org/10.1016/j.ijheatmasstransfer.2018.04.140.